Available online at www.sciencedirect.com
ScienceDirect
Journal of Colloid and Interface Science 317 (2008) 442–448
JOURNAL OF Colloid and Interface Science
www.elsevier.com/locate/jcis

Determination of the space between closed multiwalled carbon nanotubes by GCMC simulation of nitrogen adsorption

S. Furmaniak [a], A.P. Terzyk [a,*], P.A. Gauden [a], K. Lota [b], E. Frąckowiak [b], F. Béguin [c], P. Kowalczyk [d]

[a] *N. Copernicus University, Department of Chemistry, Physicochemistry of Carbon Materials Research Group, Gagarin St. 7, 87-100 Toruń, Poland*
[b] *Institute of Chemistry and Technical Electrochemistry, Poznań University of Technology, ul. Piotrowo 3, 60-965 Poznań, Poland*
[c] *CRMD, CNRS-University, 1b rue de la Férollerie, 45071 Orléans Cedex 02, France*
[d] *Division of Chemical Engineering, The University of Queensland, St. Lucia, Qld 4072, Australia*

Received 17 August 2007; accepted 24 September 2007

Available online 22 October 2007

Abstract

We present a new determination method of the porosity created by the adsorption space between closed multiwalled carbon nanotubes. Using the grand canonical Monte Carlo (GCMC) simulation of nitrogen adsorption at 77 K and applying the "Karolina" algorithm, local isotherms were simulated for different distances between parallel nanotubes and finally the equation of the global adsorption isotherm was solved. This methodology leads to a satisfactory description of the experimental nitrogen adsorption data showing that the distance between nanotubes is in the range between 4 and 14 nm.
© 2007 Elsevier Inc. All rights reserved.

Keywords: Adsorption; Carbon nanotubes; Pore-size distribution

1. Introduction

Recently, nitrogen adsorption data obtained on closed and opened multiwalled carbon nanotubes (MWNTs) were reported [1–4]. The pore-size distribution (PSD) was determined from these data using some simple methods [5]. As it was recently proved on those materials, the secondary porosity created between the tubes plays a very important role in the adsorption mechanism, even if the process takes place in opened MWNTs [5]. On the other hand, characterizing the secondary porosity created by the adsorption space between the external surfaces of MWNTs is a complicated problem [6–12]. Due to the geometry of this space, the slit-like or cylindrical models cannot be applied. Not only the distribution of different nanotube diameters should be considered for the theoretical description of adsorption in carbon nanotubes, but also the effect of imperfect lateral ordering and the adsorption in the heterogeneous interstitial channels [13,14]. In sum, adsorption outside nanotubes should also be modeled [13–27]. This study presents a method applying the results of grand canonical Monte Carlo (GCMC) simulation of nitrogen adsorption in the space between closed MWNTs. A new algorithm for solving the global adsorption isotherm (GAI) equation is tested and the pore-size distribution (PSD) is recovered from the nitrogen adsorption data.

2. Experimental: Preparation of carbon nanotubes and nitrogen adsorption measurements

A precursor of the solid solution was prepared by thoroughly mixing appropriate amounts of magnesium nitrate hexahydrate, cobalt nitrate hexahydrate, and citric acid in a minimum amount of water. After gentle evaporation of water, the viscous gel obtained was dried at 423 K and then calcined under a nitrogen flow at 973 K for 5 h, to give the $Co_xMg_{1-x}O$ solid solution. A thin layer of oxide powder on a porcelain plate was introduced into a quartz tube reactor, and the temperature was stabilized at 873 K under a nitrogen flow (350 ml/min). Then

* Corresponding author. Fax: +48 056 654 24 77.
E-mail address: aterzyk@chem.uni.torun.pl (A.P. Terzyk).
URL: http://www.chem.uni.torun.pl/~aterzyk.

0021-9797/$ – see front matter © 2007 Elsevier Inc. All rights reserved.
doi:10.1016/j.jcis.2007.09.067

acetylene was introduced at a flow rate of 100 ml/min for 1 h together with nitrogen, leading to the production of carbon nanotubes. After cooling, the catalysis substrate was dissolved by hydrochloric acid (12 mol/l) treatment at 353 K for 12 h, the solution was filtrated, and the carbon nanotubes were repeatedly washed with deionized water until neutral pH of filtrate and dried at 393 K. The details of the procedure can be found elsewhere [1,3,4].

Nitrogen adsorption isotherms were measured using an ASAP 2010 volumetric adsorption analyzer from Micromeritics (Norcross, GA) at liquid nitrogen temperature (77 K) in the relative pressure range from about 10^{-6} up to 0.999. Before the measurements, the samples were outgassed for 2 h at a temperature of 473 K.

3. GCMC simulation

For each point in the nitrogen adsorption (77 K) isotherm, 25×10^6 iterations were performed during the equilibration, and then 25×10^6 equilibrium ones were applied for the averages calculation (one iteration = an attempt of changing the state of the system by displacement, creation, or annihilation). The probabilities of state change of the systems via displacement, creation, and/or annihilation of nitrogen molecule were the same (i.e., 1/3). The energy of fluid–fluid interactions (U_{ff}) was modeled by the Lennard-Jones potential [28],

$$U_{\mathrm{ff}}(r) = 4\varepsilon_{\mathrm{ff}}\left[\left(\frac{\sigma_{\mathrm{ff}}}{r}\right)^{12} - \left(\frac{\sigma_{\mathrm{ff}}}{r}\right)^{6}\right], \tag{1}$$

with the parameters $\varepsilon_{\mathrm{ff}}/k_{\mathrm{B}} = 101.5$ K, $\sigma_{\mathrm{ff}} = 0.3615$ nm, and $r_{\mathrm{cut}} = 5\sigma_{\mathrm{ff}}$. The solid–fluid potential of the interaction of nitrogen with outer surface of a single nanotube was applied in the form derived by Tanaka et al. [29],

$$U_{\mathrm{sf}}(r, R) = \pi^2 \rho_{\mathrm{s}} \varepsilon_{\mathrm{sf}} \sigma_{\mathrm{sf}}^2 \left[\frac{63}{32}\frac{F(-\frac{9}{2}, -\frac{9}{2}, 1, \delta^2)}{((1-\delta^2)R^*)^{10}}\delta^{11} - 3\frac{F(-\frac{3}{2}, -\frac{3}{2}, 1, \delta^2)}{((1-\delta^2)R^*)^{4}}\delta^{5}\right], \tag{2}$$

where $\delta = R/r$, $R^* = r/\sigma_{\mathrm{sf}}$, and R is the tube radius, r is the distance of the nitrogen molecule from the tube center, ρ_{s} is the density of carbon atoms in the wall (38.2 nm^{-2}), $\sigma_{\mathrm{sf}} = 0.3494$ nm, $\varepsilon_{\mathrm{sf}}/k_{\mathrm{B}} = 53.22$ K, $F(a, b, c, z)$ is the four-parameter hypergeometric function given by

$$F(a, b, c, z) = 1 + \frac{ab}{c}\cdot z + \frac{1}{2!}\cdot\frac{a(a+1)(b+1)}{c(c+1)}\cdot z^2 + \cdots. \tag{3}$$

The interactions with MWNTs were taken into account by simple summation for each layer.

Fig. 1 shows the simulation box, with a parallel arrangement of nanotubes of radius $R = 6$ nm separated by a distance Δd (note that if $\Delta d = 0$ the centers of carbon atoms forming the outer tube layers are separated by the distance equal to σ; see Fig. 1). Previous TEM investigations [1] showed that this radius dominates in the studied material. The local adsorption isotherms presented in Fig. 2 were calculated for boxes having the following size (l_{box}): 17.45, 17.7, 18.0, 18.5, 19.0, 19.5, 20.0, 21.0, 22.0, 23.0, 24.0, 25.0, 26.0, 27.0, 28.0, 29.0, 30.0, 32.0, 34.0, 36.0, 38.0, 40.0, and 45.0 nm. Those sizes are related to the following distances (Δd) between nanotubes: 0.0, 0.176, 0.388, 0.741, 1.10, 1.45, 1.80, 2.51, 3.22, 3.92, 4.63, 5.33, 6.04, 6.75, 7.46, 8.17, 8.87, 10.3, 11.7, 13.1, 14.5, 15.9, and 19.5 nm. The inset in Fig. 2 shows the influence of the number of carbon layers, N_{layer} (from 1 up to 5 in each tube), on the local isotherm with a box of $l_{\mathrm{box}} = 17.45$ nm. Since the differences vanish for a number of layers larger than 3 we used the latter value in the simulations [30].

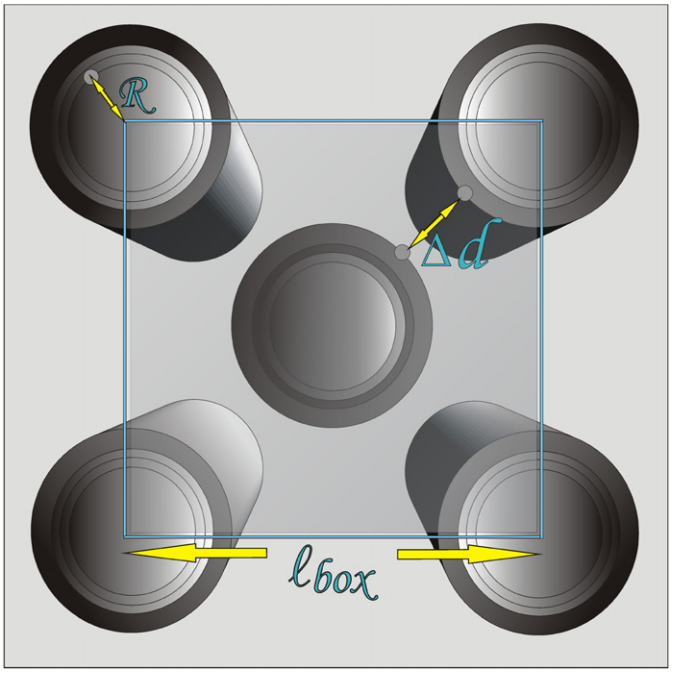

Fig. 1. The simulation box of length l_{box}. R is the distance between the nanotube center and the carbon atom center in the first layer. Δd is the distance between the outer layers of two adjacent nanotubes.

The simulated local isotherms in Fig. 2 show that the critical pore filling pressure can be successfully approximated by the Kelvin-like dependence: $\ln(p_{\mathrm{C}}/p_0) = f(l_{\mathrm{box}})$. The condensation pressure shifts toward larger values with the rise in the spacing between tubes. Fig. 3 shows selected snapshots of the boxes with adsorbed molecules (l_{box}, 17.45 and 20.0 nm, respectively; N_{layer}, 3 in each tube; p/p_0, 0.0001, 0.1, and 0.4).

4. Recovering of PSD by the "Karolina" algorithm

4.1. Basics of the algorithm

A new algorithm was constructed for recovering the PSD curves from the simulated local isotherms, θ_l (shown in Fig. 2). This new algorithm, called "Karolina" was inspired by proposed previously ASA code [31–33]; however, the applied new approach for solving of the problem makes this algorithm completely different than the ASA one. The base of "Karolina" is the application of the global adsorption isotherm (GAI) equa-

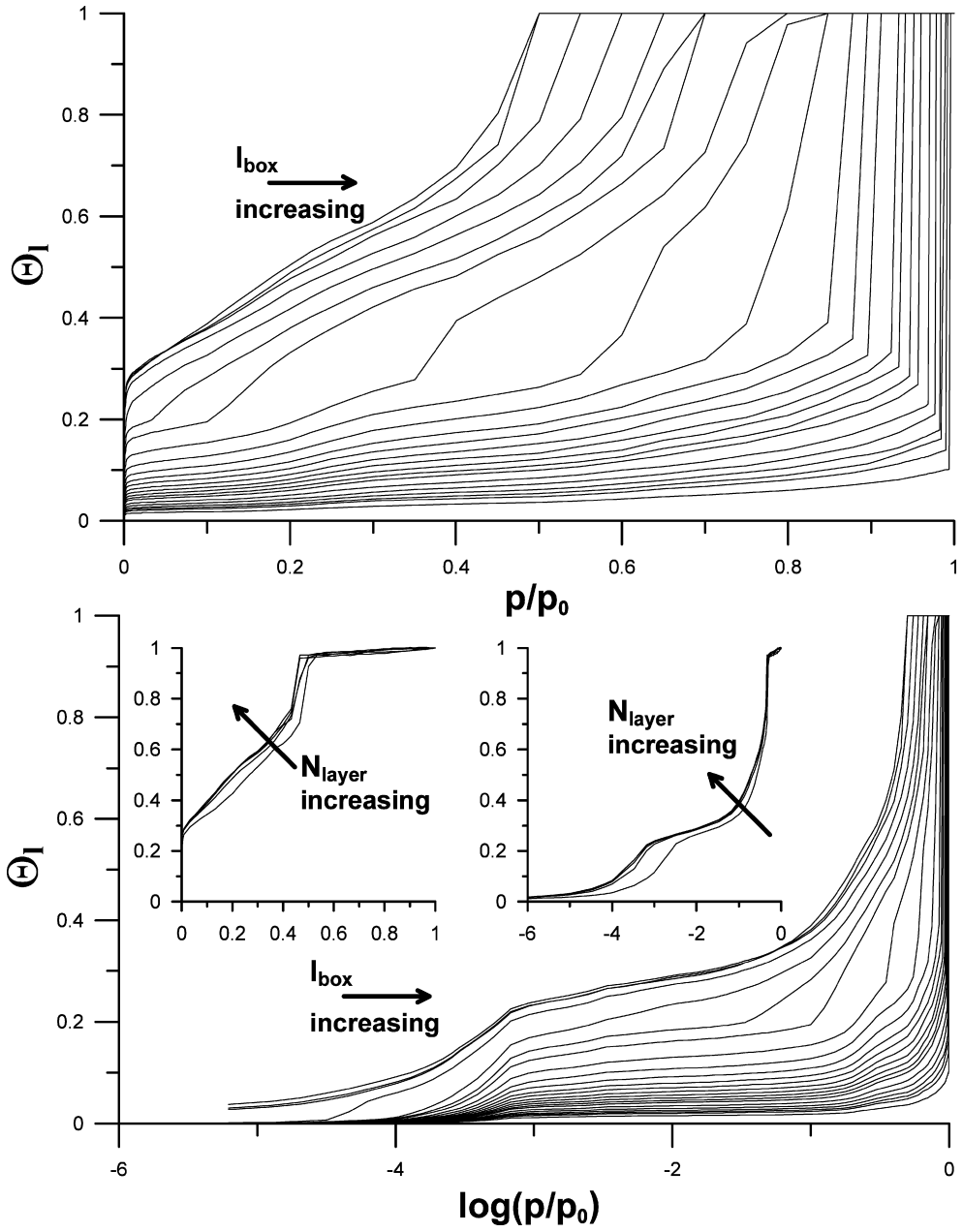

Fig. 2. Nitrogen (77 K) adsorption isotherms for closed nanotubes. Local isotherms from top to bottom $l_{box} = 17.45$, 17.7, 18.0, 18.5, 19.0, 19.5, 20.0, 21.0, 22.0, 23.0, 24.0, 25.0, 26.0, 27.0, 28.0, 29.0, 30.0, 32.0, 34.0, 36.0, 38.0, 40.0, and 45.0 nm. The inset shows the influence of the number of carbon layers, N_{layer} (from 1 up to 5 for each tube), on the local adsorption isotherms ($l_{box} = 17.45$ nm).

tion in the form of sum,

$$\Theta_l(p) = \int_{x_{min}}^{x_{max}} \Theta_l(p,x)\chi(x)\,dx = \sum_{i=1}^{N} w_i \Theta_l(p,x_i)$$
$$= \int_{\Delta d_{min}}^{\Delta d_{max}} \Theta_l(p,\Delta d)\chi(\Delta d)\,d\Delta d = \sum_{i=1}^{N} w_i \Theta_l(p,\Delta d), \quad (4)$$

where x is the structural parameter (here equal to Δd; see Fig. 1), w_i are the weights, and χ is the value of the PSD function.

The essence of the algorithm is the modification of the vector of weights to make the differences between the global adsorption values (calculated from Eq. (4)) and the values measured experimentally as small as possible. The measure of the differences is the value of the determination coefficient defined as

$$\mathrm{DC} = \frac{\sum_{i=1}^{N}(\Theta^{t}_{t,i} - \Theta^{o}_{t,i})^2}{\sum_{i=1}^{N}(\Theta^{o}_{t,i} - \overline{\Theta}^{o}_{t})^2}, \quad (5)$$

where $\Theta^{t}_{t,i}$ is the theoretical value obtained from summation of the local isotherms for ith point, $\Theta^{o}_{t,i}$ is the experimental value for ith point, and $\overline{\Theta}^{o}_{t}$ is the average value of the global experimental adsorption.

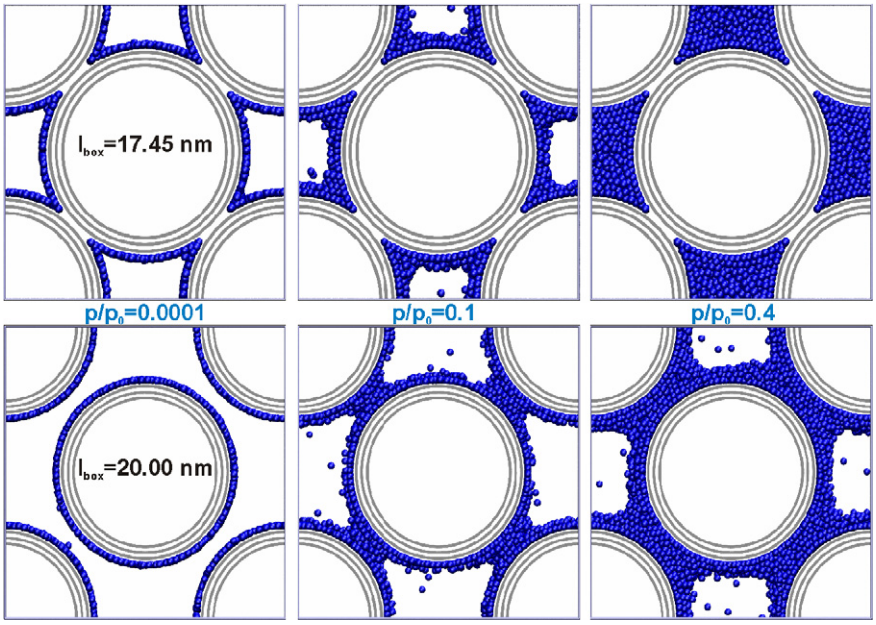

Fig. 3. Selected snapshots of equilibrium configurations generated from GCMC isotherms for $l_{box} = 17.45$ (top) and 20.0 nm (bottom), and relative pressures = 0.0001, 0.1, and 0.4 (from left to right). $N_{layer} = 3$ in each tube.

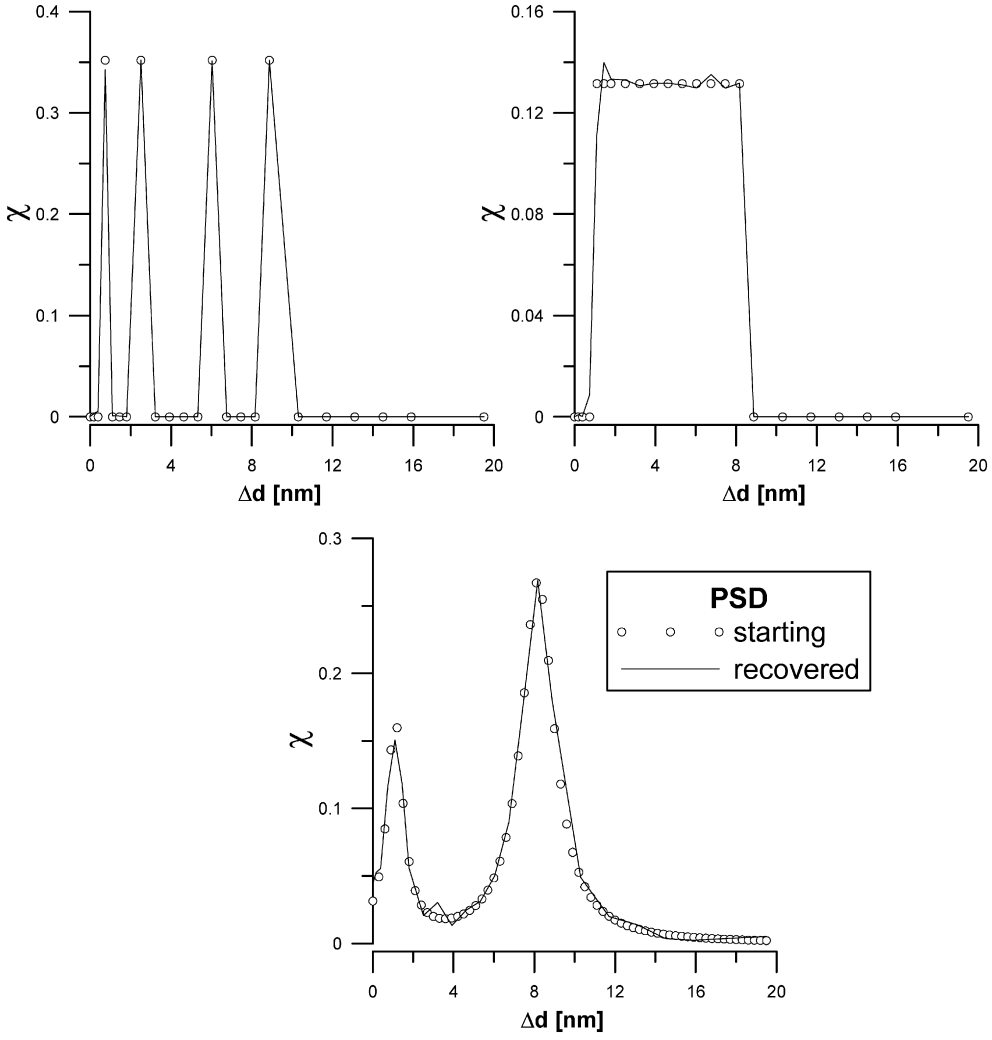

Fig. 4. Representative data showing the recovering of assumed Δd distributions by the "Karolina" algorithm.

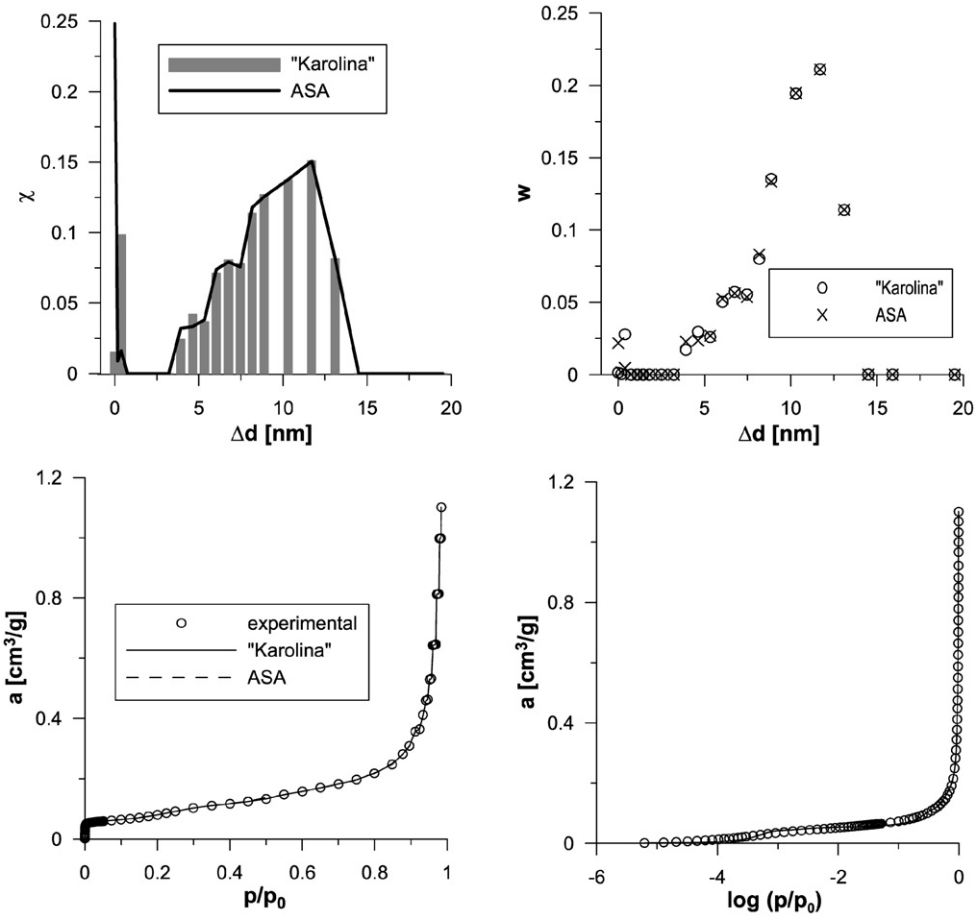

Fig. 5. The distribution of pores between closed MWNTs obtained from Eq. (4) with local GCMC isotherms using "Karolina" and ASA algorithms, together with the fit of the experimental nitrogen adsorption isotherm (77 K) (determination coefficient, $DC_{\text{"Karolina"}} = DC_{ASA} = 0.998$). The averaged results from 3 runs are shown (in each run almost the same fit was obtained).

The starting point is the assumption of the normalized vector of weights equal to all considered local isotherms. In each successive iteration the code tries to modify the vector of weights, and the number of attempts of the modifications is equal to the number of local isotherms. Such attempt is made by the random determination of the number of components of the vector of weights (from 1 up to 5), and next random choice of the position of the components of the vector of weights being modified. The procedure leading to modification of weights (10 times) leads to the random change of the chosen components (in the range -0.01 up to 0.01) and checking, at each step, if the change leads to the improvement of the DC (if not, next attempts of the modification are done (no more than 3)). Each successfully finished modification is accepted, causing the change of the chosen components of the vector w, and they become the starting point for further modification. The program stops after reaching the maximum number of iterations (10^4) or if in the defined number of following iterations (50) the value of the DC does not change more than the assumed threshold limit (10^{-10}).

4.2. Method of conversion of the vector of weights into the distribution function

The conversion of weights into the values of distribution function (χ) is done assuming the approximation of the value of integral using the trapezoidal rule of integration,

$$\begin{aligned}\Theta_t &= \int_{x_{\min}}^{x_{\max}} \Theta_l \chi \, dx \cong \sum_{i=1}^{N} w_i \Theta_{l,i} \\ &\cong \frac{1}{2} \sum_{i=1}^{N-1} (\Theta_{l,i}\chi_i + \Theta_{l,i+1}\chi_{i+1})(x_{i+1} - x_i) \\ &= \frac{1}{2}\Bigg(\Theta_{l,1}\chi_1 (x_2 - x_1) + \sum_{i=2}^{N-1} \Theta_{l,i}\chi_i (x_{i+1} - x_{i-1}) \\ &\quad + \Theta_{l,N}\chi_N (x_N - x_{N-1}) \Bigg) \end{aligned} \tag{6}$$

leading to

$$\chi_i = \begin{cases} \dfrac{2w_1}{x_2 - x_1}, & i = 1, \\ \dfrac{2w_i}{x_{i+1} - x_{i-1}}, & 1 < i < N, \\ \dfrac{2w_N}{x_N - x_{N-1}}, & i = N. \end{cases} \tag{7}$$

4.3. The basic differences between "Karolina" and ASA

The fundamental differences between both codes can be summarized as follows:

(i) "Karolina" is constructed in such a way that a simultaneous modification of a few components of the vector of weights is possible (in the ASA only one can be modified). This gives new possibilities since the change of some components can lead to a better fit only with the simultaneous modification of the other components (of course it is possible that each change performed separately does not lead to the improvement of the fit).
(ii) The components are modified in a random way (ASA makes it in turn [31–33]) and this is important if some local isotherms are similar in shapes. In the latter case using the ASA it is possible that the weight of the first isotherm can be overestimated (this situation is shown in Fig. 5).
(iii) The applied procedure makes "Karolina" faster and more stable than ASA.

5. Results and discussion

From Fig. 3 one can observe that the differences in adsorption mechanisms are determined by the distance between tubes. In the case of $l_{box} = 17.45$ nm, the high packing of the nanotubes prevents the creation of a monolayer at low pressures. When the spacing increases, a full monolayer can be created on the nanotubes. As expected, due to the strong adsorption potential, adsorption starts in the corners and on the external surfaces of MWNTs.

In Fig. 4, we present selected results of the validity test of "Karolina" algorithm. Global adsorption isotherms were generated for different a priori assumed distributions of Δd. Then, these generated global isotherms were fitted by the algorithm, allowing the PSD curves to be recovered. Fig. 4 shows a very good recovering of the assumed PSD curves, even for very complicated cases.

Fig. 5 shows a satisfactory fitting of the experimental nitrogen adsorption isotherm for closed MWNTs, with a determination coefficient equal to 0.998. We also show in this figure the comparison of the PSD obtained from the ASA algorithm using exactly the same basis of local isotherms. As one can see due to the reasons noted above the ASA code in this case overestimates the weight of the local isotherm simulated for the smallest distances between nanotubes. However, the fit between theoretical and experimental isotherms is very good for both methods. The obtained porosity distribution suggests an adsorption space with Δd distributed in the range 4–14 nm, which correlates well with previous TEM measurements [1].

6. Conclusions

The presented new method of determination of the porosity created by the adsorption space between closed multiwalled carbon nanotubes (basing on the GCMC simulations and freshly projected "Karolina" algorithm) leads to a satisfactory description of the experimental nitrogen adsorption data and shows that the adsorption space is distributed in the range 4–14 nm, which correlates well with previous TEM measurements. The proposed new algorithm of solving of the GAI equation, due to applied methodology, is fast and efficient. Moreover some artifacts originating from the similarity of the local isotherms are successfully eliminated.

Acknowledgments

S.F. and A.P.T. gratefully acknowledge the financial support from UMK Grant 350-Ch. The authors acknowledge the use of the computer cluster at Poznań Supercomputing and Networking Centre (Poland) and the Information and Communication Technology Centre of the Nicolaus Copernicus University (Toruń, Poland).

References

[1] S. Delpeux, K. Szostak, E. Frąckowiak, S. Bonnamy, F. Béguin, J. Nanosci. Nanotechnol. 2 (2002) 481.
[2] F.R. Hung, K.E. Gubbins, R. Radhakrishnan, K. Szostak, F. Béguin, G. Dudziak, M. Śliwińska-Bartkowiak, Appl. Phys. Lett. 86 (2005) 103110.
[3] E. Raymundo-Pinero, T. Cacciaguerra, P. Simon, F. Béguin, Chem. Phys. Lett. 412 (2005) 184.
[4] S. Delpeux, K. Szostak, E. Frąckowiak, S. Bonnamy, F. Béguin, Chem. Phys. Lett. 404 (2005) 374.
[5] P.A. Gauden, A.P. Terzyk, G. Rychlicki, P. Kowalczyk, K. Lota, E. Raymundo-Pinero, E. Frąckowiak, F. Béguin, Chem. Phys. Lett. 421 (2006) 409.
[6] S. Agnihotri, J.P.B. Mota, M. Rostam-Abadi, M.J. Rood, Carbon 44 (2006) 2376.
[7] S. Agnihotri, J.P.B. Mota, M. Rostam-Abadi, M.J. Rood, Langmuir 21 (2005) 896.
[8] M. Muris, N. Dupont-Pavlovsky, M. Bienfait, P. Zeppenfeld, Surf. Sci. 292 (2001) 67.
[9] J. Jiang, S.I. Sandler, Phys. Rev. B 68 (2003) 245412.
[10] J. Jiang, S.I. Sandler, M. Schenk, B. Smit, Phys. Rev. B 72 (2005) 045447.
[11] S.M. Gatica, M.M. Calbi, M.W. Cole, Phys. Rev. E 65 (2002) 061605.
[12] S. Utsumi, J. Miyawaki, H. Tanaka, Y. Hattori, T. Itoi, N. Ichikuni, H. Kanoh, M. Yudasaka, S. Iijima, K. Kaneko, J. Phys. Chem. B 109 (2005) 14319.
[13] W. Shi, J.K. Johnson, Phys. Chem. Lett. 91 (2003) 015504.
[14] M. Bienfait, P. Zeppenfeld, N. Dupont-Pavlovsky, M. Muris, M.R. Jonson, T. Wilson, M. DePies, O.E. Vilches, Phys. Rev. B 70 (2004) 035410.
[15] J. Cheng, X. Yuan, L. Zhao, D. Huang, M. Zhao, L. Dai, R. Ding, Carbon 42 (2004) 1019.
[16] K.A. Williams, P.C. Eklund, Chem. Phys. Lett. 320 (2000) 352.
[17] B.K. Pradhan, G.U. Sumanasekera, K.W. Adu, H.E. Romero, K.A. Williams, P.C. Eklund, Phys. B 323 (2002) 115.
[18] T. Ohba, K. Kaneko, J. Phys. Chem. B 106 (2002) 7171.
[19] T. Ohba, H. Kanoh, M. Yudasaka, S. Iijima, K. Kaneko, J. Phys. Chem. B 109 (2005) 8659.
[20] Ch. Matranga, L. Chen, B. Bockrath, J.K. Johnson, Phys. Rev. B 70 (2004) 165416.
[21] Z. Liu, L.-Ch. Qin, Carbon 43 (2005) 2146.
[22] P. Kowalczyk, L. Brualla, A. Żywociński, S.K. Bhatia, J. Phys. Chem. C 111 (2007) 5250.
[23] A. Fujiwara, K. Ishii, H. Suematsu, H. Kataura, Y. Maniwa, S. Suzuki, Y. Achiba, Chem. Phys. Lett. 336 (2001) 205.
[24] P. Kowalczyk, R. Hołyst, M. Terrones, H. Terrones, Phys. Chem. Chem. Phys. 9 (2007) 1786.

[25] M.M. Calbi, M.W. Cole, S.M. Gatica, M.J. Bojan, G. Stan, Rev. Mod. Phys. 73 (2001) 857.
[26] M.J. Bojan, S. Curtarolo, S.M. Gatica, M.W. Cole, Phys. Rev. B 62 (2000) 032173.
[27] P. Kowalczyk, R. Hołyst, H. Tanaka, K. Kaneko, J. Phys. Chem. B 109 (2005) 14659.
[28] D. Frenkel, B. Smit, Understanding Molecular Simulation, Academic Press, San Diego, 1996.
[29] H. Tanaka, M. El-Merraoui, W.A. Steele, K. Kaneko, Chem. Phys. Lett. 352 (2002) 334.
[30] R. Vander Wal, A.J. Tomasek, J.D. King, Carbon 43 (2005) 2918.
[31] P.A. Gauden, P. Kowalczyk, A.P. Terzyk, Langmuir 19 (2003) 4253.
[32] P. Kowalczyk, L. Solarz, A.P. Terzyk, P.A. Gauden, V.M. Gun'ko, Shedae Informaticae MCCLIX (2002) 75.
[33] P. Kowalczyk, A.P. Terzyk, P.A. Gauden, R. Leboda, E. Szmechtig-Gauden, G. Rychlicki, Z. Ryu, H. Rong, Carbon 41 (2003) 1113.